Collisionless expansion of pulsed rf plasmas I: Front formation

T Schröder,[1] O Grulke,[1] T Klinger,[1,2] R W Boswell,[3] and C Charles[3]
[1)] *Max-Planck-Institute for Plasma Physics, Greifswald, Germany*
[2)] *Ernst-Moritz-Arndt-University, Greifswald, Germany*
[3)] *Space Plasma, Power and Propulsion Group, Research School of Physical Sciences and Engineering, The Australian National University, Australian Capital Territory 0200, Australia*

The dynamics during plasma expansion are studied with the use of a versatile particle-in-cell simulation with a variable neutral gas density profile. The simulation is tailored to an rf plasma expansion experiment[1]. The experiment has shown the existence of a propagating ion front. The ion front features a strong electric field and features a sharp plasma potential drop similar to a double layer. However, the presented results of a first principle simulation show that in general the ion front does not have to be entangled with an electric field. The propagating electric field reflects the downstream ions, which stream with velocities up to twice as high as that of the the ion front propagation. The observed ion density peak forms due to the accumulation of the reflected ions. The simulation shows that the ion front formation strongly depends on the initial ion density profile and is subject to a wave-breaking phenomenon.

Virtual diagnostics in the code allow for a direct comparison with experimental results. Using this technique, the plateau forming in the wake of the plasma front could be indirectly verified in the expansion experiment. Although the simulation considers profiles only in one spatial dimensional, its results are qualitatively in very good agreement with the laboratory experiment. It can successfully reproduce findings obtained by independent numerical models and simulations. This indicates that the effects of magnetic field structures and tangential inhomogeneities are not essential for the general expansion dynamic. The presented simulation will be used for a detailed parameter study dealt with in part II of this series.

PACS numbers: 5275Di, 5259Dk, 5259Fn
Keywords: plasma acceleration, plasma expansion, PIC simulation

I. INTRODUCTION

The present work deals with dynamic structures that form during the expansion of plasma into an environment of much lower plasma density. The pressure driven electron expansion occurs on a much faster time scale than the expansion of the ions. This is owed to their higher mobility. The high inertia of the ions causes the generation of an ambipolar electric field. This electric field decelerates the escaping electrons while accelerating the ions. The ambipolar boundary propagates outwards and forms a plasma density front. For small density differences, the propagation of the front can be described with the linear ansatz of ion acoustic waves. For large density differences, experiments and simulation have shown that the propagation velocity of the density front remains proportional to the ion sound velocity. Most of these theoretical approaches have investigated the temporal evolution of an initially step-like (semi-infinite) ion density profile in collisionless, hydrodynamic regimes. They commonly evolve into self-similar density profiles[2–9]. However, the reported the proportionality factors are scattered over a wide range of values. Their value strongly depends on the considered initial and boundary conditions. The maximum expansion velocities range from the ion sound velocity c_i[2–4] up to the electron thermal velocity v_e[7,8]. Experiments carried out in thermionic discharges[10,11], fireballs[12], and laser produced plasmas[13–17] yield that the expansion velocities depend strongly on the electron energy distribution[17–21]. It is predicted that the occurrence of high energetic electrons results in enhanced ion acceleration[10,22].

In the present work a one-dimensional particle-in-cell simulation is presented. In a simplified version, the simulation is used to analyse the influence of the initial ion plasma profile on the ion front evolution for the expansion of a semi-infinite plasma into vacuum. The main goal is to benchmark the physics of the simulation against results of independent numerical models, simulations, and experiments. The complexity is thereby increased up to a self consistent simulation of the ignition of an rf plasma tailored to an existing plasma expansion experiment[1]. In contrast to the ignition with ultra-short laser pulses[13–15,17], the use of an rf source allows for an increase of the spatial dimension of the plasma expansion. This in turn enables the use of a different set of diagnostics, such a electrostatic probes and energy analysers. Since the full simulation is designed closely to an experiment[1], it can provide a deeper insight into the particle kinetics during the expansion process, in particular during the front formation. Virtual diagnostics implemented in the code are used to re-evaluate the profiles measured in the plasma expansion experiment[1]. The results are qualitatively compared with predictions from expansion theory and independent models. The generally good agreement supports the physical relevance of the presented simulation and motivates its use for a systematic parameter study presented in part II of this series.

II. THE PARTICLE-IN-CELL CODE

The particle-in-cell (PIC) code that is used in the present study is a modified version of the *Phoenix* code[23,24] which is based on the *JanuS* code[25]. It uses a Monte Carlo collision model[26] based on available ion-neutral[27,28] (elastic and charge exchange) and electron-neutral collision cross section data[29] (elastic, excitation, and ionisation).

The code is one dimensional in space and tree dimensional in velocity space. The three dimensional velocity space ensures energy conservation and a realistic treatment of the collision scheme. A spatial element resembles an infinite, homogeneous plasma plane (x, y) of thickness dz. As demonstrated by independent 2D simulations, the generation of magnetic fields is efficiently hampered by the presents of a background plasma[30]. For simplicity, the generation of magnetic fields and their influence on the particles have been neglected. An important addition to the original code is the implementation of a variable neutral gas density profile. Since the code considers only particle collisions with neutrals, the neutral gas density is the key parameter controlling the mean free paths of both species and determines the region of electron impact ionisation. The code features a modular construction with plugins for a high versatility.

The simulation results presented in this work evolve from either one out of two general setups. The first setup uses a minimum amount of plugins and is kept very simple. It is used to characterise the relaxation of different initial density profiles. The second setup uses a larger number of plugins and is much more complex. It is tailored to an existing plasma expansion experiment[1].

The expansion of a plasma is observed to be associated with an accumulation of ions near the ion front[4,7,17]. However, for the commonly considered case of an abrupt ion density drop, it has been shown that the ion density peak at the ion front forms due to a numerical effect rather than a physical phenomenon[31]. In order to quantify the effect in the simulations, the first setup of the PIC code resembles a simplified system ($L = 100\,\mathrm{mm}$, no source, no ion-neutral collisions, no electron impact collisions) with different grid sizes d$z = 100$, 10, and $1\,\mu$m. The boundary conditions are defined by a reflecting wall with Neumann condition at $z = -20\,\mathrm{mm}$ and a grounded wall (Dirichlet, $\Phi = 0$) at $z = 80\,\mathrm{mm}$. The initial condition is a homogeneous Maxwellian plasma ($T_\mathrm{e} = 1\,\mathrm{eV}$, $T_\mathrm{i} = 0$) in the source region ($z < 0$) with an ion and electron particle density of each $n_0 = 5{\cdot}10^{15}\,\mathrm{m}^{-3}$. The expansion region ($z > 0$) contains no plasma. The configurations differ by the spatial grid size dz and the shape of initial particle density profiles around the intersection of the two regions. While changing dz, the number of macro-particles in a source cell ($z \ll 0$) is kept constant at $\eta = 50$ by accordingly adjusting the macro-factor and the number of macro-particles. This way, the influence of the spatial grid size and the initial ion front shape on the front evolution can be investigated.

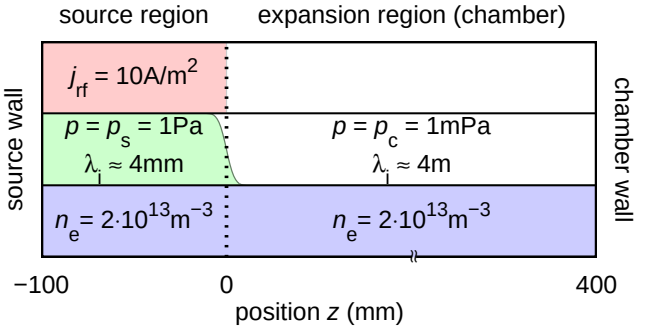

FIG. 1. Schematic of the second setup with the induced rf current density j_rf, the neutral gas pressure p, and the initial electron density n_e. λ_i is the ion mean free path.

The second setup is designed close to previous plasma expansion experiments[1] and implements similar *virtual* diagnostics. It can be used to re-evaluate the measured data obtained experimentally. The one dimensional simulation domain is divided into two regions, the source region and the expansion region. It is terminated by two grounded walls. The setup is illustrated in figure 1. In the source region an inductive rf-field j_rf ($f_\mathrm{rf} = 10\mathrm{Mhz}$) is driven, which is influencing the electron kinetics. The neutral gas pressure inside the source is increased allowing for ohmic heating of the electrons. This results in a very high rate of electron impact ionisation in the source region. The neutral gas pressure profile features a negative gradient centred around the intersection between source and expansion region as indicated in figure 1. The profile is given by:

$$p(z,t) = \frac{p_\mathrm{s} - p_\mathrm{c}}{2} \cdot \left[1 - \mathrm{erf}\left(\frac{z - v_\mathrm{n} t}{w_\mathrm{n}}\right)\right] + p_\mathrm{c}\,, \quad (1)$$

where p_s and p_c are the gas pressure levels in the source and the expansion region, respectively, w_n defines the width of the gradient, and v_n denotes the neutral drift velocity. In the expansion region the inductive field is zero. The neutral gas pressure is up to three orders of magnitude smaller than in the source allowing for a collisionless expansion of the ions. Rather than into vacuum, this setup simulates the expansion of plasma into an ambient plasma of much smaller electron density. The total domain is initially filled with a uniformly distributed background plasma of a certain small base electron density $n_\mathrm{e} = 2 \cdot 10^{13}\,\mathrm{m}^{-3}$ (blue area). The background plasma provides the first electrons required for the source mechanism to work. It also ensures the stability of the initial phase of the simulation. A set of input parameters for the reference simulation run is compiled in table I.

Remark: Under default conditions with two grounded walls, the simulation evolves a constant net current through the plasma. This net current can be suppressed by choosing at least one wall to be insulating (charge accumulating). A comparison of the two cases has shown that the general expansion mechanics is unaffected.

parameter	default value
time step	$\mathrm{t} = 10^{-10}\,\mathrm{s}$
boundary condition	DIRICHLET ($\Phi_0 = \Phi_{N_\mathrm{G}+1} = 0$)
system length	$L = 500\,\mathrm{mm}$
grid size	$N_\mathrm{G} = 5000$ ($\mathrm{d}z = 0.1\,\mathrm{mm}$)
ion mass	$m_\mathrm{i} = 40\,\mathrm{u}$ (Argon)
electron mass	$1\,m_\mathrm{e}$
macrofactor	$10^8\,\mathrm{m}^{-2}$
initial electron temp.	$T_\mathrm{e} = 0.5\,\mathrm{eV}$
initial ion temperature	$T_\mathrm{i} = 0.026\,\mathrm{eV}$ ($300K$)
initial particle count	$N_\mathrm{e} = N_\mathrm{i} = 10^5$ ($n_\mathrm{b} = 2{\cdot}10^{13}\,\mathrm{m}^{-3}$)
gas temp	$T_\mathrm{n} = 300\,\mathrm{K}$
gas pressure (source)	$p_\mathrm{s} = 1\,\mathrm{Pa}$
gas pressure (chamber)	$p_\mathrm{c} = 1\,\mathrm{mPa}$
gas front position	$z_\mathrm{n} = 0\,\mathrm{mm}$
gas front velocity	$v_\mathrm{n} = 0\,\mathrm{m/s}$
gas front width	$w_\mathrm{n} = 0\,\mathrm{mm}$
source type	rf (inductive)
source power factor	$P = 1\,P_0$
current density	$j_\mathrm{rf} = 10\,\mathrm{Am}^{-2}{\cdot}P$
source range	$-100\ldots0\,\mathrm{mm}$
source frequency	$f_\mathrm{rf} = 10\,\mathrm{MHz}$

TABLE I. The settings and initial parameters for the reference simulation run.

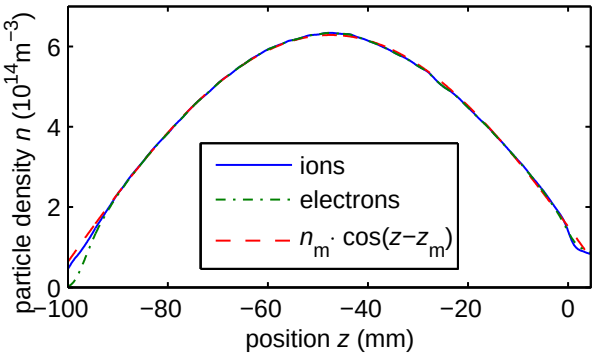

FIG. 2. Typical ion density profile of the source region in comparison with the theoretical sinusoidal profile.

A. Source profile

Being the origin of the expansion, the source region is a vital part of the second simulation setup. In the source region, plasma is created self-consistently via electron impact ionisation. The evolving plasma profiles are determined in particular by the collisionality and the boundary conditions. The source wall is absorbing and grounded. However, the intersection to the expansion region is open. The source density profiles evolving from the PIC simulation are depicted in figure 2. The ion density profile (blue) can be fitted well by a sinusoidal function (red) as described by a collisional model using

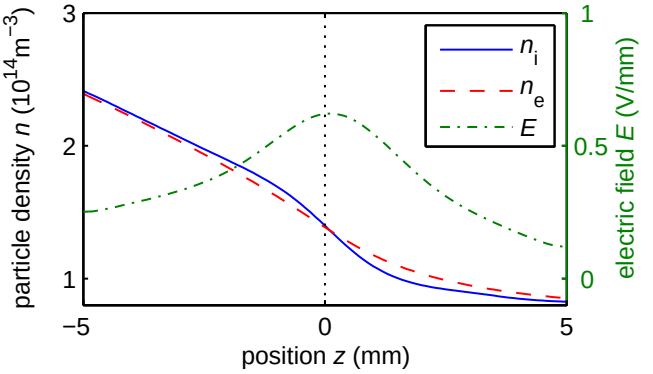

FIG. 3. Typical electron and ion density and the resulting electric field profile at the transition between source and expansion region.

the HELMHOLTZ equation

$$\nabla^2 n + \frac{\nu_\mathrm{iz}}{D} n = 0\,, \tag{2}$$

where ν_iz is the ionization frequency and D the ambipolar diffusion coefficient[32].

The plasma density evolves as if the intersection with the expansion region is given by an imaginary sheath edge. The source plasma can be considered as independent of the events in the expansion region[33]. The particle density and electric field profiles (n_i, n_e, E_z) in the region around the intersection are depicted in figure 3. The dotted line marks the intersection of source and expansion region. The electron and ion densities separate in the pre-sheath. The surplus of positive charge leads to a strong increase of the electric field. The resulting ion acceleration causes a thinning of the ion density. The profiles eventually reach a point, at which the ion density drop due to acceleration is larger than the electron density drop due to repulsion. The local charge density $\varrho = e(n_\mathrm{i} - n_\mathrm{e})$ decreases again and finally changes sign near the intersection. At this point the electric field has reached its maximum and starts to decrease. The ion drift velocity has reached the BOHM velocity. The potential drop from the edge potential to the plateau level is on the order of the electron temperature $\Delta\Phi \approx k_\mathrm{B}T_\mathrm{e}/e$. Consequently, the plateau ion velocity and the plateau front velocity is supersonic. Together with the BOHM velocity, the kinetic energy of the plateau ions can roughly be estimated to $E_\mathrm{kin} \approx \frac{3}{2}k_\mathrm{B}T_\mathrm{e}$.

III. SIMULATION RESULTS: ION FRONT SHAPES

In order to investigate the influence of the spatial grid size on the density profile evolution, three different configurations are used considering the cases $\mathrm{d}z > \lambda_\mathrm{D}$, $\mathrm{d}z < \lambda_\mathrm{D}$, and $\mathrm{d}z \ll \lambda_\mathrm{D}$ (λ_D: DEBYE length). The ion density n_i and the electric field E_z profiles of each configuration are shown in figure 4 as red and green curves,

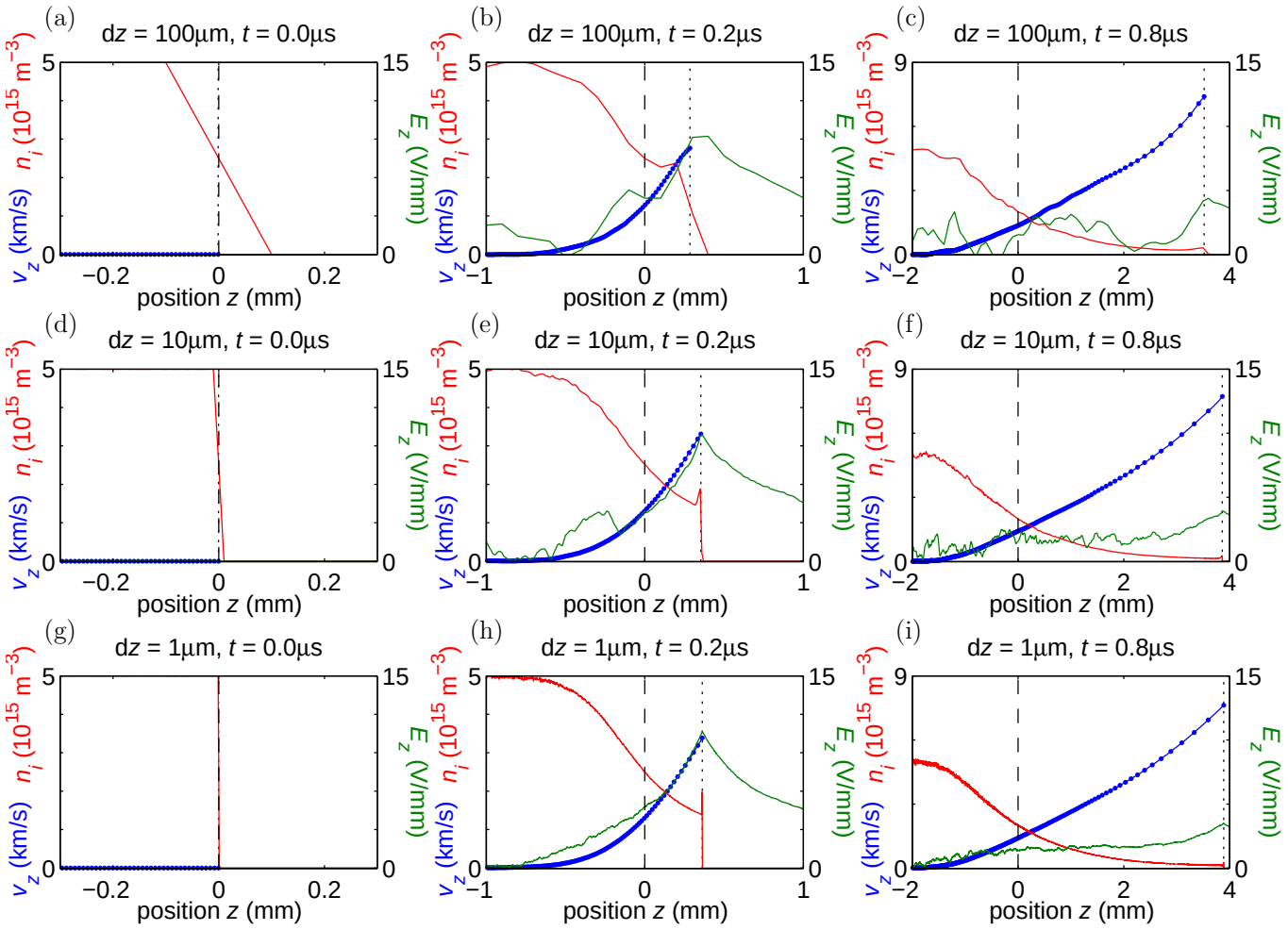

FIG. 4. The ion phase space (blue), the ion density (red), and the electric field (green) for three different grid sizes dz (rows) at three time instants t (columns).

respectively. Each configuration (rows) is represented by three time instants t of the simulation run (columns). The initial condition ($t = 0$) is depicted in the first column. The blue bullets represent initially equally spaced sample ions in phase space. The position of the front is defined by the rightmost ion and is marked by the dotted line.

As the simulation evolves, the density front progresses to the right. The ion density is continuously decreasing with increasing z. In the vicinity of the front, the ion density profile has a local maximum before dropping to zero. The detailed profile of the ion density profile strongly depends on the grid size dz. The width of the ion density peak at the front edge for $t = 0.2\,\mu$s (second column in figure 4) scales monotonically with dz. This indicates a numerical artefact caused by a too low spatial resolution. The electric field increases and reaches its maximum just at the front edge. The proper profile of the electric field near the front is of a higher order and not properly resolved by the linear interpolation used in the particle pusher. The electrostatic force in cells upstream of the front is overestimated by the interpolation due to the positive curvature of the electric field profile. Conversely, in the cell that covers the front, the electrostatic force is underestimated. This prevents the ion density at the front from decreasing and leads to the formation of the peak. The ion peak density at the front decreases over time (right column in figure 4) and is always lower than the main plasma density in the source region. For a non-zero ion temperature T_i, the influence of this numerical effect is attenuated. For $\mathrm{d}z < v_{\mathrm{th_i}}/f_{\mathrm{p_i}}$ ($v_{\mathrm{th_i}}$ denotes the ion thermal velocity and $f_{\mathrm{p_i}}$ the ion plasma frequency), the ion density peak is no longer observed. This is in contrast to the expansion of plasma with an initially finite ion density drop[31,34,35] or to expansion into an ambient plasma[9,36,37].

The front formation for initially finite ion density gradients is shown in figure 5. The spacing of the plotted sample ions is adapted to their local density. The plots show three time instants of two different initial ion density profiles, a linear front and smooth profile following an arc cotangent function. The initial profiles are shown

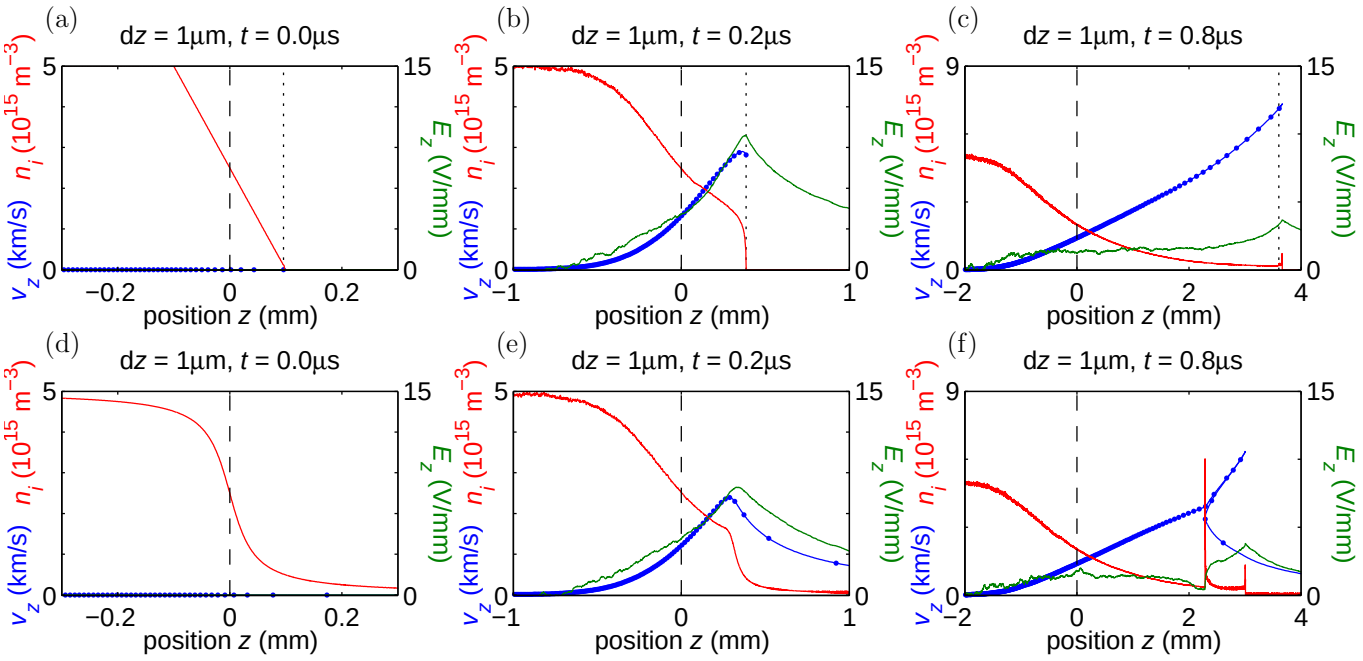

FIG. 5. The ion phase space (blue), the ion density (red), and the electric field (green) at three time instants t for (a–c) a linear and (d–f) a smooth, inverse cotangential ion density drop.

in figure 5a and figure 5d, respectively. Both simulation runs show that the maximum of the electric field is located near the maximum gradient of the ion density profiles ($t = 0.2\,\mu$s). The lower half of the front ions experiences a negative electric field gradient. The acceleration of the ions towards the electric field maximum is larger compared to the acceleration of the ions located further downstream. They become faster and eventually will overtake the slower ones. This behaviour results in a local ion density increase. Within a few ion plasma oscillation periods $t = 0.8\,\mu\text{s} > 10/\omega_{\text{p}_\text{i}}$ the fast ions have overtaken the slower ones and form the ion burst. After this wave-breaking event, the two initial profiles evolve differently: For a linear profile, the burst ions are the right-most ions located at the maximum electric field. All ions near the front experience a positive electric field gradient leading to a thinning of the front ion density. The ion density profile asymptotically approaches the solution for the abrupt ion density drop. The propagation velocity of the ion burst is constantly increasing and can be many times the ion sound velocity. The temporal evolution of the ion burst velocity for the smooth ion density profile is shown in figure 7a (blue). For a smooth ion density profile, there are always ions in the region of the negative electric field gradient. The electric field is strong enough to reflect the downstream ions. For cold-ions there is a well defined turning point, where the ions have been accelerated to the propagation velocity of the electric field. The turning point features a second local ion density maximum. The electric field upstream of the maximum vanishes and propagates with an approximately constant velocity being much smaller than the ion burst velocity. The temporal development of the propagation velocity of the turning point is shown in figure 7b (blue).

This mechanism can also be observed during the plasma expansion into an ambient plasma. Figure 6 shows the profiles for a configuration of an ambient plasma with the density $n_\text{a} = 0.1\,n_0$ in the positive half space ($z > 0$). The negative electric field gradient downstream of the ion front causes the ambient ions to accumulate as the front approaches. The general behaviour is in good agreement with numerical results of a cold-ion model[9]. In contrast to the continuous ion profile (figure 5d), the ambient plasma has a homogeneous plasma density and the density of the ions reflected by the electric field remains constant. The ion density profile upstream of the turning point decreases over time and, eventually, is comparable to the ambient plasma density. The ion density becomes critical and wave-breaking occurs, i.e. upstream ions overtake downstream ions (dotted line). After longer times, the plasma density upstream of the of the turning point (second peak) saturates and forms a plateau.

The front of the plateau (turning point) corresponds to the propagating double layer that has been observed in independent plasma expansion experiments[10]. The commonly discussed ion front, however, is actually formed by the ion burst. In the cold-ion limit, the plateau density shows oscillations similar to the ones described by the cold-ion model[9]. The temporal evolution of the burst velocity and the velocity of the turning point are shown in figure 7a and figure 7b (red), respectively. Compared to the smooth ion density gradient, the acceleration of the

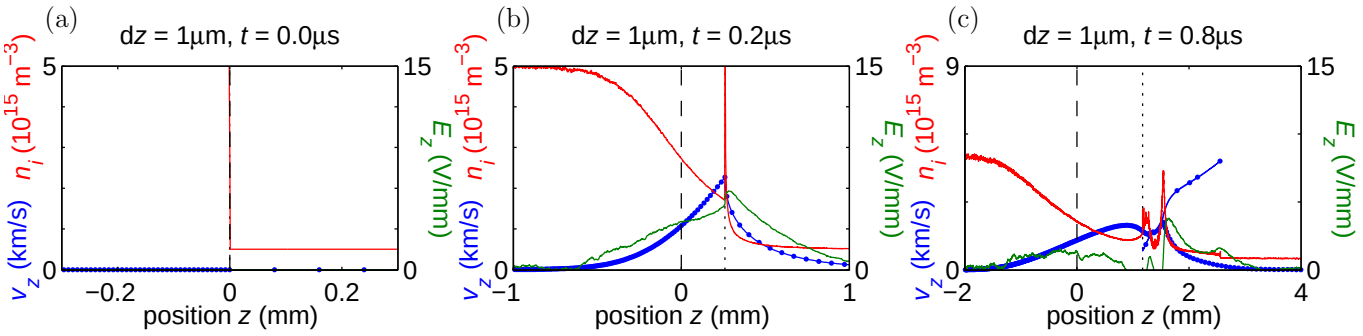

FIG. 6. The ion phase space (blue), the ion density (red), and the electric field (green) at three time instants t for the plasma expansion into an ambient plasma.

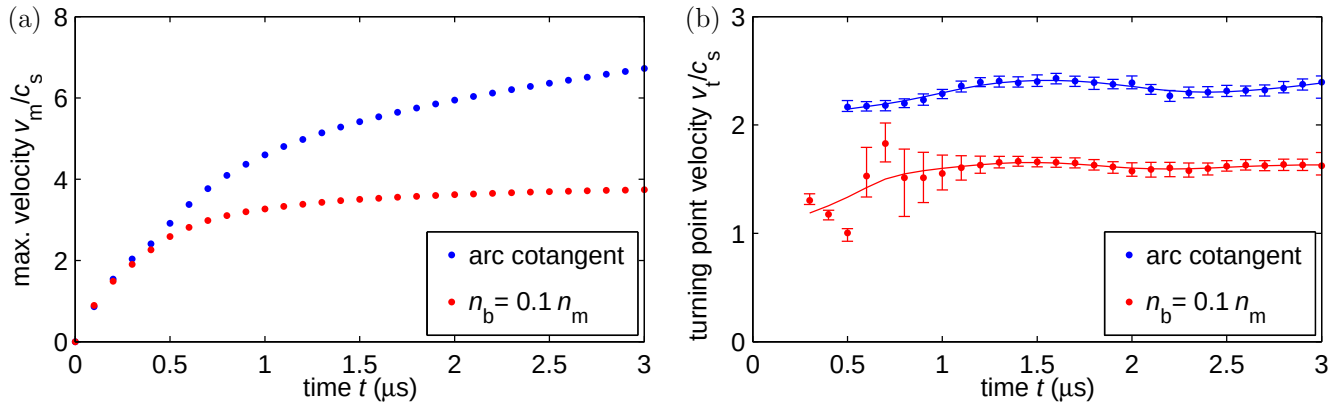

FIG. 7. (a) Maximum ion velocity vs. time. (b) Propagation velocity of the turning point vs. time. The blue and red data sets correspond to the initially smooth ion density drop (arc cotangent) and the initial condition with an ambient plasma of the density $n_\mathrm{b} = 0.1\, n_\mathrm{m}$, respectively.

burst is significantly reduced and the velocity saturates at $v_\mathrm{b} \approx 4\, c_\mathrm{s}$. The propagation velocity of the turning point is smaller at $v_\mathrm{t} \approx 1.6 c_s$.

For a density ratio close to unity, the electric field at the plateau front is not strong enough to reflect the ambient ions. In this case, the plasma expansion problem reduces to the propagation of small density perturbations. This situation is well understood in the framework of ion acoustic waves[38].

For a finite ion density drop, the presence of an ambient plasma, or a finite ion temperature, the numerical artefact is insignificant and can be neglected.

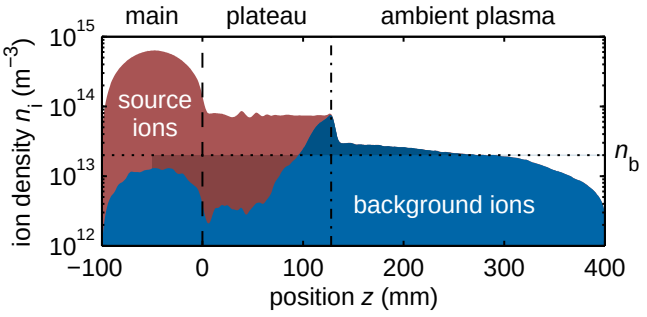

FIG. 8. Source ions (red) mainly govern main and plateau plasma. The ambient plasma is almost exclusively formed by background ions (blue) from the initialisation. The profile is a sample at $t = 30\mu$s

IV. SIMULATION RESULTS: PLASMA EXPANSION

The expansion process as computed by the simulation has some common features. A typical axial plasma density profile is depicted in form of an area plot in figure 8. The ion density is presented on a logarithmic scale against the axial position z after a simulated time of $t = 30\,\mu$s. Initially, the simulation domain is homogeneously filled with background plasma of the plasma density n_b (dotted line). By electron impact ionisation, source ions are introduced in the source region triggering the expansion. The total plasma density profile is separated into two sub-profiles given as colour coded areas. The blue area represents the background ions and the red area represents the source ions created by electron impact ionisation.

One can distinguish between the main, the plateau,

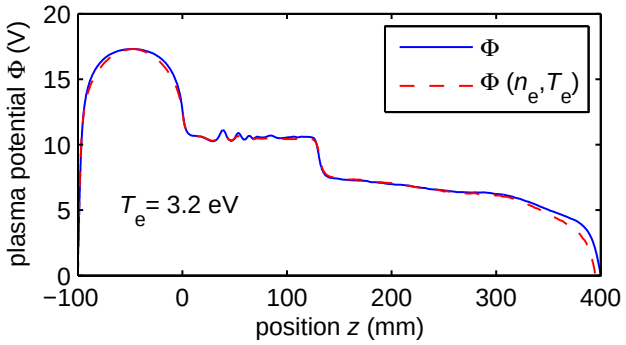

FIG. 9. The plasma potential profile (blue) compared with the plasma potential obtained from BOLTZMANN's relation (red).

and the ambient plasma, separated by the dashed ($z \approx 0$) and dash-dotted line ($z \approx 130\,\mathrm{mm}$), respectively. This separation has been reported for independent one- and two-dimensional PIC simulations[36,37], in which, however, the plateau is less pronounced. These simulations also predict the formation of a rarefaction wave that is propagating upstream. In the present simulation, the rarefaction is suppressed by the plasma generation due to electron impact ionisation. The plasma density reaches its maximum of $n_\mathrm{m} \approx 6.4{\cdot}10^{14}\,\mathrm{m}^{-3}$ near the centre of the source region. Its source profile can be approximated by the collisional model given by Eqn. (2). The plateau plasma has an intermediate, approximately constant density. Its intersection with the ambient plasma features a significant plasma density gradient. The background ions show a small density increase with an approximately constant gradient near the plateau front. Beyond $z \approx 300\,\mathrm{mm}$, the density deviates from n_b due to a sheath and pre-sheath formation ($\lambda_\mathrm{D} \approx 3\,\mathrm{mm}$) in front of the chamber wall ($z = 400\,\mathrm{mm}$).

Due to the much higher neutral gas pressure, electron impact ionisation predominantly occurs in the source region. Source ions that have been ionized near the intersection propagate into the plateau. The resulting electric field structure repels the background ions. In figure 8 this is illustrated by the darkened areas. The displaced background ions accumulate near the intersection of the plateau and ambient plasma. They form the front of the plateau. The background ions are partially reflected by this front and enter the ambient plasma in form of an ion stream. Some of the background ions in the source region ($z < -50\,\mathrm{mm}$) are lost at the source wall. The profile of the corresponding plasma potential Φ is depicted in figure 9. It is compared with the plasma potential calculated from the electron density profile n_e using the BOLTZMANN's relation:

$$e\Phi = e\Phi_\mathrm{m} + k_\mathrm{B} T_\mathrm{e} \ln\left(\frac{\mathrm{n_e}}{\mathrm{n_m}}\right), \qquad (3)$$

where Φ_m is the maximum plasma potential and $T_\mathrm{e} \approx 3.2\,\mathrm{eV}$ the electron temperature. The so obtained electron temperature is in good agreement with the electron temperature obtained from the electron velocity distribution function. Thus, the potential drop at the plateau front is not a double layer in the strict sense[39]. However, the observation of a double layer has been reported for the expansion of a thermionic discharge[40].

A. Ion velocity distribution function

The ion velocity distribution functions obtained by the PIC simulation are depicted in figure 10 for three different time instants. The illustrations show the characteristic triangular shape of the phase space in the early phase (a) and a decelerated ion population (red circle) at later times (b) and (c), respectively. The final structure after wave-breaking is shown in figure 10c. It shows the separation of the plateau around $z = 20\,\mathrm{mm}$ into two regions of different mean velocity and ion temperature. The source side ions of the plateau are faster and stream into the vortex. In the vortex the drift velocity is converted into thermal energy of the ions in the chamber side region. At the plateau front, a stream of ions is flowing into the ambient plasma with the velocity $v_\mathrm{s} \approx 2v_\mathrm{f}$. The end of the stream consists of an ion population that is even faster. It has been launched during the wave-breaking event. This ion burst (blue ellipsis in figure 10c) has a wide velocity spread that is tearing it apart. Its maximum velocity is $v_\mathrm{b} \approx 10.5\,\mathrm{km/s}$. The additional acceleration of the burst has been reconstructed by a simple simulation of a propagating electric field[1]. The ion stream is contributing to the ambient plasma density and explains the plasma density increase in figure 8. Given by BOLTZMANN's relation, the plasma density increase affects the local plasma potential and increases sightly the accelerating electric field.

For comparison, the ion and electron density profiles are shown in figure 11 for the respective time instances. At $t = 2\,\mu\mathrm{s}$ (a), the ion density shows a pronounced local maximum at the location where the wave-breaking takes place ($z \approx 5\,\mathrm{mm}$). This maximum is entangled with the wave-breaking process (ion collapse[41,42]) and predicted by a number of models[4,7,17,31,34,35] The electron density is in equilibrium and has an exponential profile. After the wave-breaking event (b), the peak of the ion density becomes broader and splits into two maxima of similar amplitude, but different velocity. The downstream peak ($z_\mathrm{v} \approx 13\,\mathrm{mm}$) corresponds to the plateau front, whereas the upstream peak ($z_\mathrm{f} \approx 10\,\mathrm{mm}$) is due to the decelerated ion population (red circle in figure 10b). The electron density profile follows the ion density increase and shows the onset of the plateau. The plateau density becomes smaller over time and the exponential drop at the plateau front becomes steeper (c). The two peaks ($z_\mathrm{v} \approx 20\,\mathrm{mm}$, $z_\mathrm{f} \approx 40\,\mathrm{mm}$) in the ion density profile get separated and delimit a region of approximate constant ion density.

The temporal evolution of the ion velocity probabil-

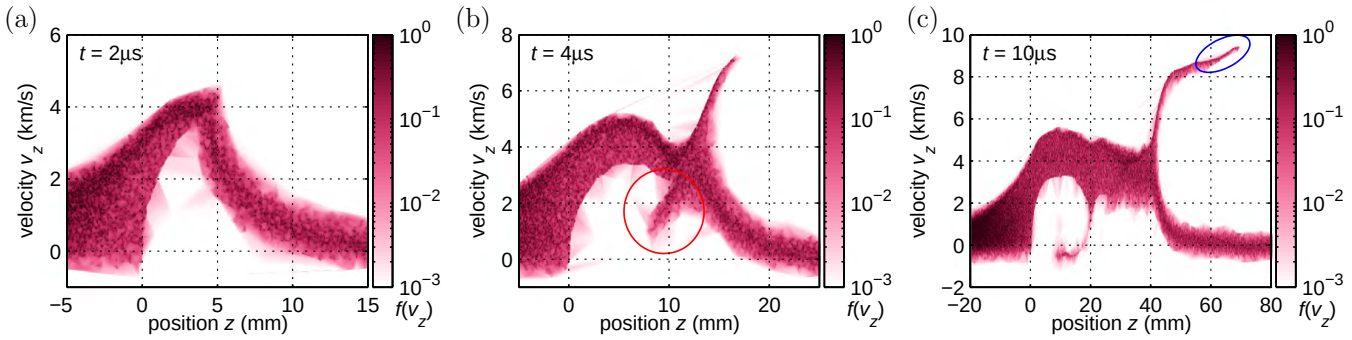

FIG. 10. Ion velocity distribution functions near the ion front at different simulation times (a–c).

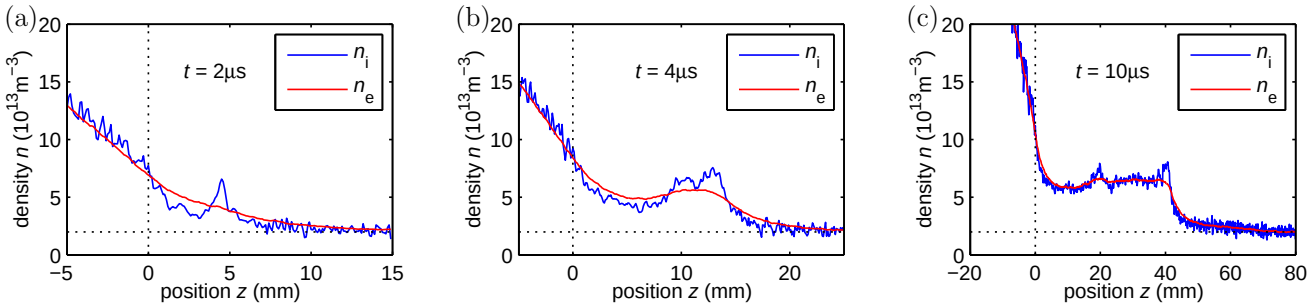

FIG. 11. Ion n_i (blue) and electron density profiles n_e (red) near the ion front at different simulation times (a–c).

ity density (IVPD), is presented in figure 12. The graph displays an isosurface in position z, time t, and velocity v_z of the ion velocity probability density f_v. The isovalue of the surface is a fraction of the maximum value $f_{v_\mathrm{iso}} = 10^{-3} f_{v_\mathrm{max}}$. Thereby, the majority of the populated phase space enclosed by the surface. In order to provide information of the inner distribution, the caps of the graph, i.e. the front and left hand sides of the graph, are colour coded in shades of red according to the respective ion velocity probability density. The isosurface itself is colour coded according to the velocity. The origin is defined by the intersection of source and expansion region ($z = 0$), the time the source is turned on ($t = 0$), and the average velocity of the initial ions ($v = 0$).

The illustration shows, how the ions propagate into the expansion region. The expansion profile can be separated into three populations/regions. They are well separated by the colour tone of the surface. The ambient and source ions without drift are covered in blue, a broad ion stream forming the plateau in green and the fast ion stream and ion burst in orange and red, respectively. The source ions have a small velocity as they are generated out of the neutral gas population at room temperature with a drift velocity of $v_\mathrm{n} = 0$ in the default setup. The peaked plasma potential profile in the source region creates an accelerating electric field for ions pushing them out of the source centre. Thus, the ion velocity is increasing towards the edges of the source ($z = 0\,\mathrm{mm}$). The plateau forms at the edge of the ionisation region and propagates with a constant average velocity ranging from $z \approx 0\,\mathrm{mm}$ at $t \approx 0\,\mu\mathrm{s}$ to $z \approx 130\,\mathrm{mm}$ at $t = 30\,\mu\mathrm{s}$. The average propagation velocity is $v_\mathrm{f} \approx 4.4\,\mathrm{km/s}$. The propagation can easily be traced either by following the sharp edge of the front itself or by the local minimum of the drift velocity. The minimum is located just behind the front as indicated by the blue dotted line. The plateau front features a narrow area of strong acceleration of the ambient ions. They are reflected by the plateau front (blue dashed line) and form an energetic ion stream marked by the solid blue ellipsis. The velocity gain is approximately twice the front velocity. In the early phase ($t < 0.3\,\mu\mathrm{s}$), the ion acceleration is higher due to a sharper plasma density gradient. This results in a burst of even faster ions marked by the blue dash-dotted ellipsis. The velocity spread in the ion burst tears it apart and results in a flattening in phase space. Consequently, the burst is much more pronounced in the early phase. Over time, it becomes less distinguishable from the ion stream.

Downstream of the vortex, the ion temperature is increased. Probable candidates for the heating mechanism are plasma drift instabilities[43]. In result, the ion velocity distribution offers an easy way to locate the vortex. The red dashed line marks the position of the ion temperature increase. This position is also entangled with a local maximum of the ion drift velocity and can be tracked in time as shown by the red dotted line. The ions that are decelerated in the vortex remain at a positive drift velocity. They form a second ion population marked by the red ellipsis. This is in good agreement with the numerical solutions of a Vlasov-Poisson model[9]. The

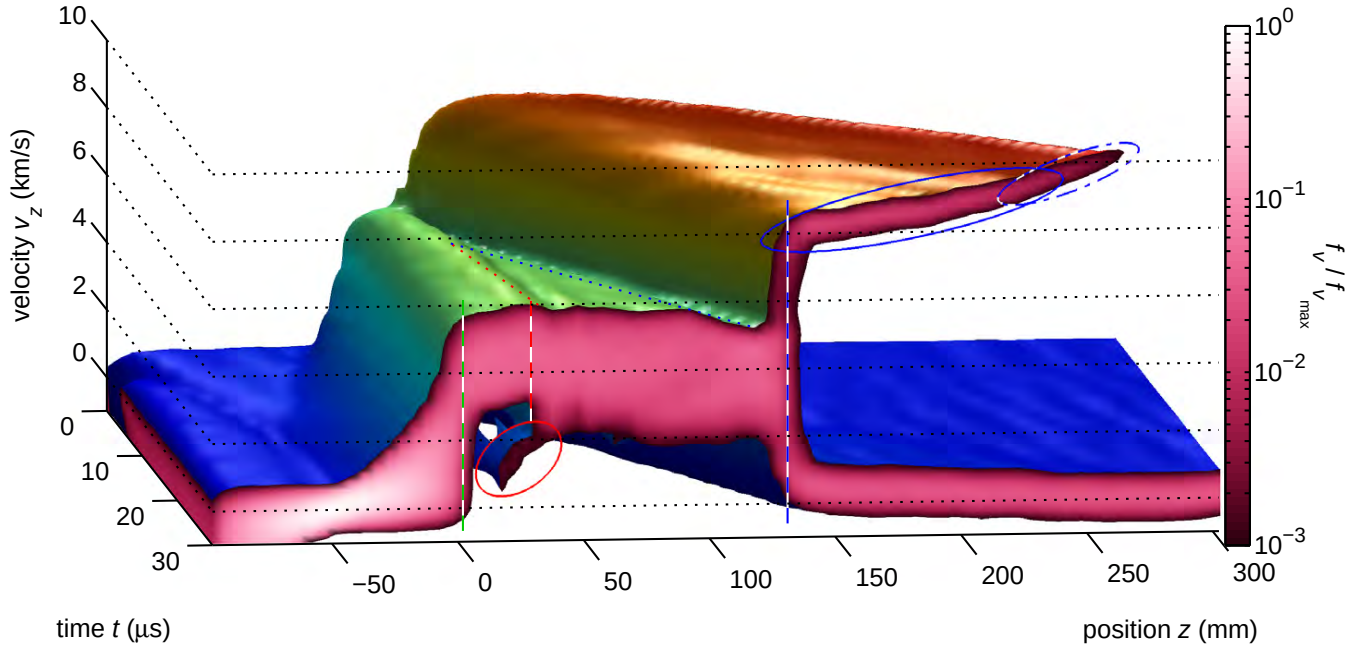

FIG. 12. Isosurface plot of the IVPD for the default setup with enhanced particle resolution. The features are emphasised by the coloured lines and ellipses.

electron velocity distribution function is featureless apart from the trivial change of the temperature along z due to the potential drops.

B. Comparison with the experiment

Although the simulation is tailored to the experimental situation, numerical issues prevent a quantitative match of the plasma parameters, in particular the electron density. Nevertheless, the temporal evolution of the parameter profiles show a qualitatively good agreement with the experimental data[1]. One very important feature of the experimental data is the strong discrepancy of the measured ion and electron saturation currents near the front. Assuming the measured probe currents are proportional to the particle densities, their discrepancy should generate an enormous electric field. Since no evidence of such a strong electric field has been found, the discrepancy is presumably generated by non-thermal electrons and ions. From the data generated by the PIC simulation, a virtual diagnostic tool can calculate the net current to a virtual LANGMUIR probe with arbitrary biasing. A comparison of the saturation current profiles with the respective density profiles is depicted in figure 13.

For a better comparability of the two saturation currents and the particle densities, the profiles have been normalised. The densities of ions and electrons are almost identical apart from the structural differences pointed out in A (c.f. Fig 11). The electron current follows the electron density quite well. The small de-

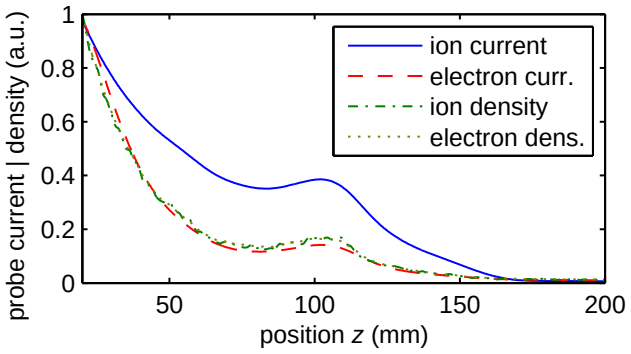

FIG. 13. Ion and electron currents in comparison to the normalised ion and electron density profiles using virtual diagnostics for $t = 20\,\mu$s.

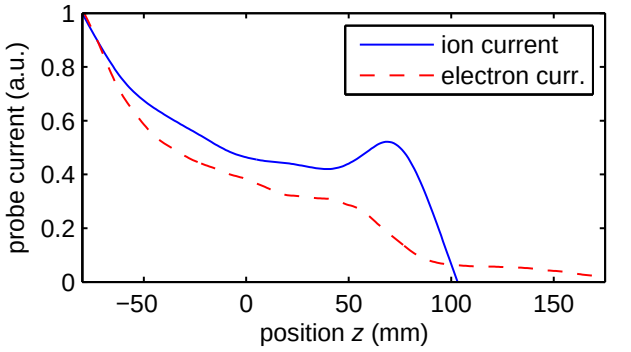

FIG. 14. Ion and electron currents from the plasma expansion experiment for $t \approx 570\,\mu$s (c.f. Ref. [1], Figure. 10).

viations are mainly related to the electron temperature profile.

In case of the ions, the current and density profiles show significant discrepancies. Its slope in the transition to the plateau is much more shallow than the slope of the density profiles. In the transition to the plateau the discrepancy grows until the ion current profile reaches a small local maximum close to the front. The maximum is related to the turning point discussed in section III. The current drawn in the ion saturation regime is influenced by the sonic and supersonic drifts of the ion populations in the plateau and stream, respectively. The drift enhances the ion current to the probe. This will lead to an overestimation of the plasma density if LANGMUIR's probe theory is applied. A similar discrepancy has been observed in the experimental data[1] depicted in figure 14.

The plot shows the measured ion and electron current profiles during the plasma expansion. Both profiles are normalised to their respective maxima ($z = -75\,\mathrm{mm}$). The ion current profile has a local maximum ($z = 70\,\mathrm{mm}$). Although this maximum is much more pronounced, both profiles are qualitatively in good agreement with the PIC simulation. This indicates that the simulation includes all relevant mechanisms that have a notable impact on the observed plasma expansion. The local ion current increase is predominantly related to a change of the plasma potential. Nevertheless, the simulation shows that ion density does form a localised maximum near the front. This is in good agreement with observations in laser plasma expansion experiments[44]. The inversion of the ion current beyond the front could not be reproduced, which is presumably due to the much higher background density in the simulation.

V. SUMMARY AND CONCLUSION

This paper has presented a study on expanding plasma. The expansion of plasma is characterised by a sharp density gradient associated with strong electric fields as given by the BOLTZMANN relation. The electric field accelerates the ions in the direction of the expansion (downstream) and a propagating ion front is formed. Such propagating fronts have been found to play a key role in the generation of non-thermal particle populations[45,46]. They have have been observed in various plasma discharges, e.g. thermionic[10], laser[15,16,47–49], arc plasmas[13,50], and rf-discharges[1]. The determination of the propagation velocity of ion fronts is ambiguous. There are different types of ion fronts that can form. In particular, one has to distinguish between the expansion into vacuum and into ambient plasma. The influence of the ambient plasma on the plasma expansion and the ion front formation has been studied using a versatile particle-in-cell (PIC) simulation tailored to the setup of an rf plasma expansion experiment[1]. This offers the possibility to directly compare the experimental data with the simulation and to get a deeper understanding of the particle kinetics.

The plasma expansion into vacuum has been subject of a large number of analytical and numerical models and particle simulations[2–7,17,22,31,34,35,41]. The typical initial conditions are a semi-infinite ion density profile and MAXWELLian electrons. Investigations using a LAGRANGEian model have revealed that the expansion of plasma into vacuum features the generation of a slow and a fast propagating ion density peak resulting from a wave-breaking event[34]. The wave-breaking mechanism and the resulting formation of the two ion density peaks have been confirmed with the presented PIC simulation. The simulation shows that the wave-breaking event is an inevitable consequence of the negative electric field gradient affecting the downstream ions. However, after the wave-breaking event has occurred, the fast ion peak eventually dominates the local ion density and determines the location of the electric field maximum. Consequently, the expanding ions experience a positive electric field gradient leading to a continuous thinning of their density. The plasma expansion into vacuum asymptotically approaches the well-known self-similar solution[3] in which the velocity of the ion front, i.e. the fast ion peak, indefinitely increases. The simulation shows this behaviour, in good agreement with a hydrodynamic description of the expansion[5,31].

In contrast to the vacuum expansion, the plasma expansion into an ambient plasma features the formation of a stable plateau in the wake of the slow ion peak and a saturation of the ion peak velocities. The plateau is clearly observed in the PIC simulation and qualitatively in good agreement with the results form independent investigations using a VLASOV-POISSON model[9]. It is also observed in the collisionless plasma expansion experiment[1], where it can be identified indirectly by comparing the experimental results with virtual diagnostics of the PIC simulation.

The plateau is a region of approximately constant density that intersects with the main plasma by forming a vortex in ion phase space. The vortex limits the propagation velocity of the expanding ions coming from the source. This results in the constant ion drift velocity throughout the plateau. The ion drift causes two-stream instabilities[43]. In the PIC-simulation runs with cold ions ($T_\mathrm{i} = 0$), these instabilities become apparent as macroscopic ion density perturbations. They can be qualitatively described by a cold-ion model[9]. For warm ions $T_\mathrm{i} > 0$ the instabilities lead to an ion temperature increase in the plateau, which is clearly observed as a broadening of the ion velocity distribution function. The ion density profile of the plateau is more homogeneous and matches the solution of a simplified quasi-neutral cold-ion model[8,9]. For larger ratios between the main and the ambient plasma density, the vortex is propagating downstream, and the plateau becomes less pronounced. The expansion of a semi-infinite plasma into an ambient plasma with high density ratios ($n_\mathrm{m}/n_\mathrm{a} = 100$) has been investigated independently using a different PIC simula-

tion with periodic boundaries[36]. The shortening of the plateau and the transition to the vacuum case is found in both PIC simulations. A rarefaction-wave is not observed if the source module in our simulation is preventing its propagation. The agreement of the relative front velocities in both simulation approaches indicates that the rarefaction-wave is an independent mechanism. In analytical models[7] this is reflected in the constant electron density and ion drift velocity at the origin.

The intersection between the plateau and the ambient plasma is given by a sharp density drop, the plateau front. The plateau front evolves from the slow ion peak and propagates with a velocity approximately equal to the plateau drift velocity. The sharp density gradient is accompanied by a strong plasma potential gradient and resembles a propagating current-free double layer as observed in pulsed thermionic discharges[40]. However, the present PIC simulation shows that the plasma expansion mechanism requires the ion front neither to be a double layer nor current-free. The presence of a second hot electron population can amplify the potential drop at the front, and hence it can trigger a double layer formation[51]. Evidence for such a hot electron population has been found in the collisionless plasma expansion experiments[1], but the limitations of the diagnostic did not allow for a characterisation of the observed potential gradient. With respect to the plasma expansion mechanism, the PIC simulation provides no evidence for a direct influence of the current-free character.

The propagating electric field structure that is associated with the plateau front is accelerating the ambient ions while it passes through. The ions that are reflected form a narrow ion stream with stream velocities up to twice as high as the propagation velocity of the front, similar to the Fermi acceleration mechanism[45]. The ion stream is tipped by the ion burst resembling the fast ion peak, i.e. the ion front in the vacuum expansion. The ion burst density is gradually decreasing due to its velocity spread and eventually becomes negligible compared to the ambient plasma density. The electric field at the ion burst vanishes resulting in a saturation of the ion burst velocity. The maximum velocity of the ion burst can be much higher than the ion stream velocity as it is determined by the maximum potential gradient. This qualitatively confirms observations that have been made with an independent PIC simulations[36], however, with different saturation values for the burst velocity. The much sharper potential gradient in that semi-infinite PIC simulation is presumably the reason for the 60% velocity increase compared to the present results. The collisionless plasma expansion experiment provides evidence for the existence of the ion stream in the form of a propagating front[1]. The ion energy analyser in the experiment has clearly shown two different drift velocities downstream and upstream of the plateau front. The respective drift velocities match with the expected values for the ion front and ion stream velocity within a relative error of only 10%. The comparison of the front and stream velocities with the results from a Vlasov-Poisson model[9] shows that both approaches agree quantitatively within a deviation of much less than 10%.

The generally good agreement with both, the expansion experiments and the results form numerical models and simulations, validates the physical relevance of the present simulation with respect to important plasma expansion mechanisms. Based on this work, an extensive parameter study will be carried out in part II of this series.

ACKNOWLEDGMENTS

The author would like to thank the DAAD (German Students Exchange Service) for funding and the colleagues of the RSPE, ANU, Canberra for their support and hospitality.

This work has been carried out within the framework of the EUROfusion Consortium and has received funding from the European Unions Horizon 2020 research and innovation programme under grant agreement number 633053. The views and opinions expressed herein do not necessarily reflect those of the European Commission.

[1] T. Schröder, O. Grulke, T. Klinger, R. W. Boswell, and C. Charles. *J. Phys. D: Appl. Phys.*, 47(5):055207, 2014.
[2] P. Mora and R. Pellat. *Phys. Fluids*, 22(12):2300–4, 1979.
[3] A. V. Gurevich, I. V. Pariiska, and L. P. Pitaevskii. *Sov. Phys. JETP*, 22(2):449–54, 1966.
[4] M. Widner, I. Alexeff, and W. D. Jones. *Phys. Fluids*, 14(4): 795–6, 1971.
[5] P. Mora. *Phys. Rev. Lett.*, 90(18):185002, 2003.
[6] P. Mora. *Phys. Rev. E*, 72(5):056401, 2005.
[7] J. E. Crow, P. L. Auer, and J. E. Allen. *J. Plasma Phys.*, 14(1): 65–76, 1975.
[8] J. E. Allen and J. G. Andrews. *J. Plasma Phys.*, 4:187–94, 1970.
[9] M. Perego, P. D. Howell, M. D. Gunzburger, J. R. Ockendon, and J. E. Allen. *Phys. Plasmas*, 20(5):052101, 2013.
[10] G. Hairapetian and R. L. Stenzel. *Phys. Rev. Lett.*, 61(14):1607–10, 1988.
[11] G. Hairapetian and R. L. Stenzel. *Phys. Fluids B*, 3(4):899–914, 1991.
[12] R. L. Stenzel, C. Ionita, and R. Schrittwieser. *Plasma Sources Sci. Technol.*, 17(3):035006, 2008.
[13] H. W. Hendel and T. T. Reboul. *Phys. Fluids*, 5(3):360–2, 1962.
[14] G. M. W. Kroesen, D. C. Schram, A. T. M. Wilbers, and G. J. Meeusen. *Contrib. Plasma Phys.*, 31(1):27–42, 1991.
[15] Y. Kuramitsu, Y. Sakawa, T. Morita, C. D. Gregory, J. N. Waugh, S. Dono, H. Aoki, H. Tanji, M. Koenig, N. Woolsey, and H. Takabe. *Phys. Rev. Lett.*, 106:175002, 2011.
[16] H. Ahmed, M. E. Dieckmann, L. Romagnani, D. Doria, G. Sarri, M. Cerchez, E. Ianni, T. Kourakis A. L. Giesecke, M. Notley, R. Prasad, K. Quinn, O. Willi, and M. Borghesi. *Phys. Rev. Lett.*, 110:205001, 2011.
[17] A. V. Gurevich and A. P. Meshcherkin. *Sov. Phys. JETP*, 53(5): 1810–26, 1981.
[18] B. Bezzerides, D. W. Forslund, and E. L. Lindman. *Phys. Fluids*, 21(12):2179–85, 1978.
[19] J. S. Pearlman and R. L. Morse. *Phys. Rev. Lett.*, 40(25):1652–5, 1978.
[20] J. Denavit. *Phys. Fluids*, 22(7):1384–92, 1979.
[21] A. V. Mordvinov, V. M. Tomozov, and V. G. Fainshtein. *J. Appl. Mech. Tech. Phys.*, 26(6):764–8, 1985.
[22] M. A. True, J. R. Albritton, and E. A. Williams. *Phys. Fluids*, 24(10):1885–93, 1981.

[23]T. Lafleur and R. W. Boswell. *Phys. Plasmas*, 19023508, 2012.
[24]T. Lafleur, R. W. Boswell, and J. P. Booth. *Appl. Phys. Lett.*, 100194101, 2012.
[25]A. Meige, R. W. Boswell, C. Charles, and M. M. Turner. *Phys. Plasmas*, 12(5):052317, 2005.
[26]V. Vahedi and M. Surendra. *Comput. Phys. Commun.*, 87(1-2): 179–98, 1995.
[27]A. V. Phelps. *J. Phys. Chem. Ref. Data*, 20(3):557–573, 1991.
[28]A. V. Phelps. *J. Appl. Phys.*, 76(2):747–53, 1994.
[29]http://dpc.nifs.ac.jp/DB/IEEJ/. Recommended electron collision cross sections. Japanese Report 853, Institute of Electrical Engineers of Japan, Sep 2001.
[30]G. Sarri, M. E. Dieckmann, I. Kourakis, and M. Borghesi. *Phys. Rev. Lett.*, 107:025003, 2011.
[31]C. Sack and H. Schamel. *Phys. Rep.*, 156(6):311–95, 1987.
[32]M. A. Lieberman and A. J. Lichtenberg. *Principles of Plasma Discharges and Material Processing*, volume 2. Wiley, 2 edition, 2005. ISBN 0-471-72001-1.
[33]D. Bohm. *Characteristics of electrical discharges in magnetic fields*. McGraw - Hill, New York, 1949. ASIN: B000H747U0.
[34]T. Grismayer and P. Moras. *Phys. Plasmas*, 13(3):032103, 2006.
[35]J. E. Allen and M. Perego. *Phys. Plasmas*, 21(3):034504, 2014.
[36]G. Sarri, M. E. Dieckmann, I. Kourakis, and M. Borghesi. *Phys. Plasmas*, 17(8):082305, 2010.
[37]G. Sarri, G. C. Murphy, M. E. Dieckmann, A. Bret, K. Quinn, I. Kourakis, M. Borghesi, L. O. C. Drury, and A. Ynnerman. *New J. Phys.*, 13:073023, 2011.
[38]J. E. Allen and A. D. R. Phelps. *Rep. Prog. Phys.*, 40(11):1305, 1977.
[39]L. P. Block. *Astrophys. Space Sci.*, 55(1):59–83, 1978.
[40]G. Hairapetian and R. L. Stenzel. *Phys. Rev. Lett.*, 65(2):175–8, 1990.
[41]C. Sack and H. Schamel. *Plasma Phys. Control. Fusion*, 27(7): 717–49, 1985.
[42]C. Sack and H. Schamel. *Phys. Lett. A*, 110(4):206–12, 1985.
[43]R. Chodura, G. Bardotti, and F. Engelman. *Plasma Phys.*, 13 (12):1099–110, 1971.
[44]D. W. Koopman. *Phys. Fluids*, 15(1):56–&, 1972.
[45]E. Fermi. *Phys. Rev.*, 75:1169–1174, 1949.
[46]L. O'C. Drury. *Rep. Prog. Phys.*, 46(8):973–1027, 1983.
[47]S. C. Wilks, A. B. Langdon, T. E. Cowan, M. Roth, M. Singh, S. Hatchett, M. H. Key, D. Pennington, A. MacKinnon, and R. A. Snavely. *Phys. Plasmas*, 8(2):542–9, 2001.
[48]L. Romagnani, S. V. Bulanov, M. Borghesi, P. Audebert, J. C. Gauthier, K. Löwenbrück, A. J. Mackinnon, P. Patel, G. Pretzler, T. Toncian, and O. Willi. *Phys. Rev. Lett.*, 101:025004, 2008.
[49]G. Sarri, M. E. Dieckmann, C. R. D. Brown, C. A. Cecchetti, D. J. Hoarty, S. F. James, R. Jung, I. Kourakis, H. Schamel, O. Willi, and M. Borghesi. *Phys. Plasmas*, 17(1):010701, 2010.
[50]P. Vankan, S. Mazouffre, R. Engeln, and D. C. Schram. *Phys. Plasmas*, 12(10):102303, 2005.
[51]C. Chan, N. Hershkowitz, and K. E. Lonngren. *Phys. Fluids*, 26 (6):1587–95, 1983.